Catal Lett (2012) 142:408–416
DOI 10.1007/s10562-012-0799-z

Study of Oxygen Reactivity in $La_{1-x}Sr_xCoO_{3-\delta}$ Perovskites for Total Oxidation of Toluene

R. Pereñíguez · J. L. Hueso · F. Gaillard · J. P. Holgado · A. Caballero

Received: 9 January 2012 / Accepted: 3 March 2012 / Published online: 17 March 2012

Abstract The total oxidation of toluene is studied over catalytic systems based on perovskite with general formula $AA'CoO_{3-\delta}$ (A = La, A′ = Sr). The systematic and progressive substitution of La^{3+} by Sr^{2+} cations in the series ($La_{1-x}Sr_xCoO_{3-\delta}$ system) of the perovskites have been studied to determine their influence in the final properties of these mixed oxides and their corresponding reactivity performance for the total oxidation of toluene as a model volatile organic compound with detrimental effects for health and environment. The structure and morphology of the samples before and after reaction have been characterized by XRD, BET and FE-SEM techniques. Additional experiments of temperature programmed desorption of O_2 in vacuum and reduction in H_2 were also performed to identify the main surface oxygen species and the reducibility of the different perovskites. It is remarkable that the $La_{1-x}Sr_xCoO_{3-\delta}$ series presents better catalytic performance for the oxidation of toluene, with lower values for the T_{50} (temperature of 50 % toluene conversion) than the previously studied $LaNi_{1-y}Co_yO_3$ series.

Keywords Perovskites · Toluene · Total oxidation · Spray pyrolysis

R. Pereñíguez (✉) · J. L. Hueso · J. P. Holgado · A. Caballero (✉)
Instituto de Ciencia de Materiales de Sevilla (CSIC-Universidad de Sevilla) and Departamento de Química Inorgánica, Universidad de Sevilla, Avda. Américo Vespucio, 49, 41092 Seville, Spain
e-mail: rosa@icmse.csic.es

A. Caballero
e-mail: caballero@us.es

Present Address:
J. L. Hueso
Instituto de Nanociencia de Aragón (INA) y Departamento de Ingeniería, Química de la Universidad de Zaragoza, C/Mariano Esquillor s/n, Edificio I+D+I, 50015 Zaragoza, Spain

F. Gaillard
IRCELYON, Institut de recherches sur la catalyse et l′environnement de Lyon, University of Lyon-CNRS, UMR5256. Ave. Albert Einstein 2, 69626 Villeurbanne, France

1 Introduction

Toluene is a representative example of volatile organic compound (VOC) extensively used in industrial processes for the production of polymers, adhesives, petroleum derivatives or as solvent. Nevertheless, the emission of toluene from stationary and mobile sources represents a serious environmental issue due to its deleterious health effects, the easiness for spreading throughout the atmosphere and its contribution to global warming and photo smog processes [1–4]. Therefore, the control and remediation of VOCs in general, and toluene in particular, has acquired a paramount importance in the legislation of developed countries including more restricting and severe emission levels.

Heterogeneous catalytic oxidation is a well-studied alternative for the abatement of VOCs not requiring such high temperatures as thermal decomposition or extra disposal costs as carbon adsorption processes [4]. Noble-metals (supported or unsupported) are the most widespread catalysts employed in the VOC remediation. However, their use presents several drawbacks: high price, tendency to poison and sinter and sometimes poor thermal stability [1–8]. For these reasons, other alternatives have been studied during the past years. Among them, it is worth mentioning the use of photocatalysts [9] and different mixed oxides containing transition metals [2, 10, 11].

Perovskites can be also considered as a particular type of mixed oxides containing rare-earth and transition metals. They have been extensively studied due to their relative low cost, high thermal stability and good catalytic properties in oxidation processes [12–17].

Previous studies of the oxidation of toluene in the presence of lanthanum based perovskites are available on the literature. The influence of the partial substitution of cations with different oxidation states within the ($AA'BB'O_{3\pm\delta}$) perovskite network [5, 7, 15, 18–23] and the use of different supports to increase the overall surface area of the catalyst have been the main approaches achieved in previous studies [6, 24]. In a prior study [15], our group has determined how the partial substitution of Ni by Co in the lanthanum perovskite strongly affects the oxidation capability of the samples. Herein, we have also systematically evaluated the partial substitution in A-sites (Sr instead of La) of some cobalt perovskite systems prepared by spray pyrolysis. This synthesis method is feasible for scaling up, highly reproducible and operates in a single step and at moderate temperatures in comparison with sol-gel or ceramic techniques [12, 20, 22, 25]. The influence of the progressive substitution on the physical–chemical properties of the perovskites and their catalytic response towards the total oxidation of toluene has been thoroughly monitored by different techniques. Temperature programmed oxygen desorption (TPD-O_2) and hydrogen reduction (TPR-H_2) techniques have been used to shed light on the nature of the oxygen species participating in the reaction, as well as to propose a mechanism by correlating the catalytic activity with the lability of the oxygen species on the perovskite surface. X-ray diffraction (XRD) diagrams and field emission scanning electron microscopy (FE-SEM) images taken before and after reaction allowed us to complete the physical–chemical characterization of the perovskites and envision some of the reasons for the different reactivity behaviour.

2 Experimental

2.1 Synthesis of the Perovskites

The perovskite catalysts studied were prepared by means of the spray pyrolysis method using the experimental set-up previously described [12, 15, 25]. It starts from a precursor aqueous solution (0.05 M) of the nitrate salts containing $La(NO_3)_3{\cdot}6H_2O$ (99.99 %, Aldrich), $Sr(NO_3)_2$ (>99 %, Fluka) and $Co(NO_3)_2{\cdot}6H_2O$ (>98 %, Fluka), mixed in different molar ratios according to the desired stoichiometry ($LaCoO_3$, $La_{0.75}Sr_{0.25}CoO_3$ and $La_{0.5}Sr_{0.5}CoO_3$). The reactor consists of a quartz tube divided into two independent temperature zones. The solution is introduced in the reactor as aerosol particles in suspension, with an air current forced by a suction pump located at the end of the system. In the first furnace at 250 °C, the solvent (distilled water) was evaporated and the dissolved nitrates were decomposed subsequently in the second one at 600 °C, producing an initially amorphous perovskite powder. The material was collected by a porous frit of quartz located in the outlet of the heating system. Finally, the amorphous powders were calcined in air at 600 °C for 4 h, thus obtaining a crystalline structure.

2.2 Catalysts Characterization Techniques

2.2.1 XRD

The XRD analysis of the samples before and after reaction were carried out in a Siemens D-500 Diffractometer, with a Bragg–Brentano configuration and using Cu Kα radiation ($\lambda = 1.5418$ Å). The XRD data were collected in the range $2\theta = 20$–$70°$, with a step of 0.05° and an acquisition time of 1 s for each point. Particle size values were calculated by means of the Scherrer equation applied to the (0 2 4) plane at 47°.

2.2.2 BET Specific Surface Area Measurements

Specific surface areas were determined by BET isotherms carried out with N_2 adsorption–desorption curves at −196 °C in a Micromeritics model ASAP 2010. The samples were previously degassed at 200 °C for 2 h.

2.2.3 FE-SEM

The SEM images for representative samples before and after reaction have been recorded in a field emission scanning electron microscope (FE-SEM) model S-5200, working with an acceleration voltage of 5 kV.

2.2.4 Temperature Programmed Reduction (TPR-H_2)

Temperature Programmed Reduction (TPR-H_2) experiments were done in a fixed-bed quartz U-shaped reactor under a continuous flow of 50 ml min^{-1} of Ar/H_2 (5 %) heated at a constant rate of 10 °C min^{-1} from room temperature to 800 °C, according to the experimental conditions described elsewhere [26]. The hydrogen consumption and the possible products formation have been followed by a mass spectrometer (QMS-422 from Baltzers) and a thermal conductivity detector (TCD) previously calibrated with a CuO reference sample.

2.2.5 Oxygen Temperature Programmed Desorption Experiments (O_2-TPD vacuum)

Temperature Programmed Desorption of O_2 (TPD-O_2) experiments were carried out on a VGgas smart-IQ+

system equipped with a quadrupolar mass spectrometer and an independent pumping system described elsewhere [27–29]. The catalyst (100 mg) was placed in a cylindrical quartz sample holder hanged in vacuum by K-type thermocouple wires (50 μm in diameter, spot-welded onto the sample holder) in the centre of a cylindrical quartz reactor. Heating was carried out by a high-frequency system (1.1 MHz, 6 kW, CFEI, France) with a 6-turn inductive coil placed around the reactor. This system allowed a fast heating minimizing the temperature gradient of the sample holder which is thermally (except radiation mode) and mechanically isolated from both the reactor and the heating device. The reactor was previously evacuated down to 10^{-6} mbar at room temperature. Subsequently, the catalyst was heated up with lineal ramping of 20 °C min^{-1} up to a maximum temperature of 500 °C in the presence of 100 mbar of pure O_2. After adsorption for 30 min, the sample holder was cooled down and degassed at 10^{-5} mbar. Finally, desorption of O_2 was carried out up to 800 °C with a heating rate of 20 °C min^{-1}.

2.3 Catalytic Tests

The catalytic oxidation of toluene was carried out in a fixed-bed quartz U-shaped reactor operating at atmospheric pressure and using 200 mg of perovskite (sustained between quartz-wool). The reactor was placed vertically in the centre of an electric furnace electronically controlled and provided with another thermocouple. Mixture of reaction consisted of 500 ppm of toluene, O_2 (20 %) and He (balance) for a total flux of 100 ml min^{-1} thereby resulting an apparent gas hourly space velocity (GHSV) of 30,000 l kg^{-1} h^{-1}. The evolution of the reactants and products was controlled by a Perkin-Elmer Clarus 500 gas chromatograph (GC) equipped with a thermal conductimetry detector (TCD). The experiments were run at a heating rate of 1 °C min^{-1} up to 600 °C keeping constant this latter temperature for 6 h until the system was cooled down. The temperature was controlled by a chromel–alumel thermocouple placed at the catalyst position.

The T_{50} values, shown in Table 1 and Fig. 6, are defined as the temperature at which 50 % conversion of Toluene is achieved and the Specific Reaction Rate (SRR) was calculated as the reaction rate (converted mol of reactive/second) related to the specific surface area (BET m^2/g) and the mass of the catalyst employed (g).

3 Results

3.1 Morphological and Structural Characterization of the Perovskites

XRD diagrams of the $La_{1-x}Sr_xCoO_{3-\delta}$ samples are shown in Fig. 1. The depicted diffractograms correspond to the samples after 4 h of calcination at 600 °C. The data reveal that all the samples crystallize as a perovskite phase with rhombohedral symmetry according to the ICSD database. The degree of crystallinity varies within the range of the different samples. The non-substituted perovskite ($LaCoO_3$, Fig. 1a) shows pure and well-defined rhombohedral perovskite. However, Fig. 1b–c shows how the partial substitution of La by Sr in the $La_{1-x}Sr_xCoO_{3-\delta}$ system leads to a progressive decrease in the peaks intensities, related with a reduction of crystallite size in the samples. According to Scherrer adjustments for the (024) reflection in the XRD patterns (47°), the size of the nano-crystalline domains is slightly diminished (Table 1) from 32 to 13 nm. In parallel with these changes, the specific surface area of the perovskites is significantly increased by the progressive substitution of La by Sr, yielding values from 6 up to 13 m^2 g^{-1}, in the most strontium-substituted cobaltite (Table 1). SEM images of the as calcined $LaCoO_3$ sample are presented in Fig. 2. The other samples in the series present similar SEM images. The spray pyrolysis preparation method inherently leads to the formation of

Table 1 Specific surface area (BET) and particle size, activity for toluene oxidation and H_2 consumptions calculated from TPR experiments of the different lanthanum based perovskites under study

Samples	BET[a] (m^2 g^{-1})	Particle size[b] (nm)	O_2 desorbed ($\mu mol_{O2}/g_{CAT}$)		H_2 uptake ($mmol_{H2}/g_{CAT}$)	T_{50}[c] (°C)	SRR_{220}[d] (10^{-9}mol s^{-1} m^{-2})
			1^{TPD}	2^{TPD}			
$LaCoO_3$	5.7	32	97	68	6.3	219	16.2
$La_{0.75}Sr_{0.25}CoO_{3-\delta}$	10.2	16	236	236	6.5	212	11.6
$La_{0.5}Sr_{0.5}CoO_{3-\delta}$	12.8	13	342	446	6.7	218	7.5

[a] Perovskites after calcination at 600 °C

[b] Determined from Scherrer equation at (0 2 4) diffraction peak

[c] Temperature of 50 % toluene conversion

[d] Specific reaction rate at 220 °C

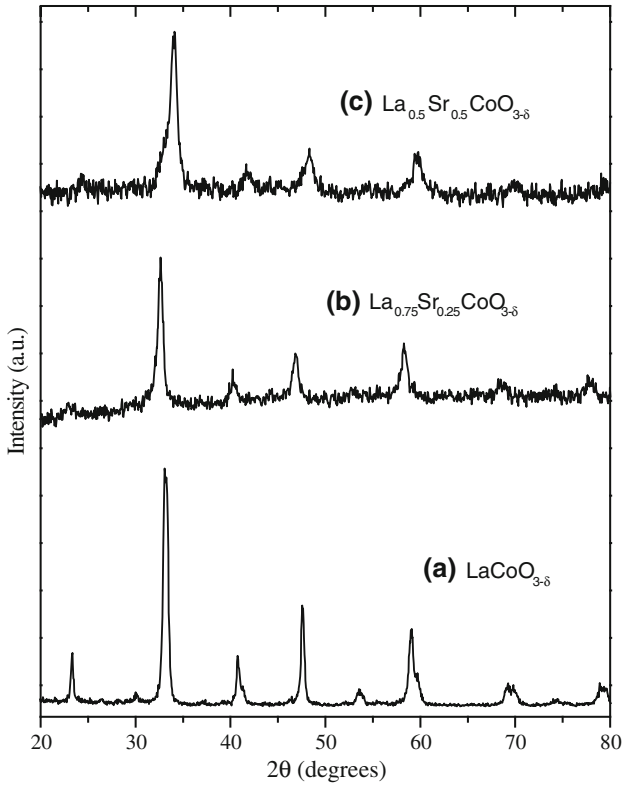

Fig. 1 XRD patterns corresponding to the different perovskites with rhombohedral symmetry: **a** $LaCoO_3$; **b** $La_{0.75}Sr_{0.25}CoO_{3-\delta}$; **c** $La_{0.5}Sr_{0.5}CoO_{3-\delta}$

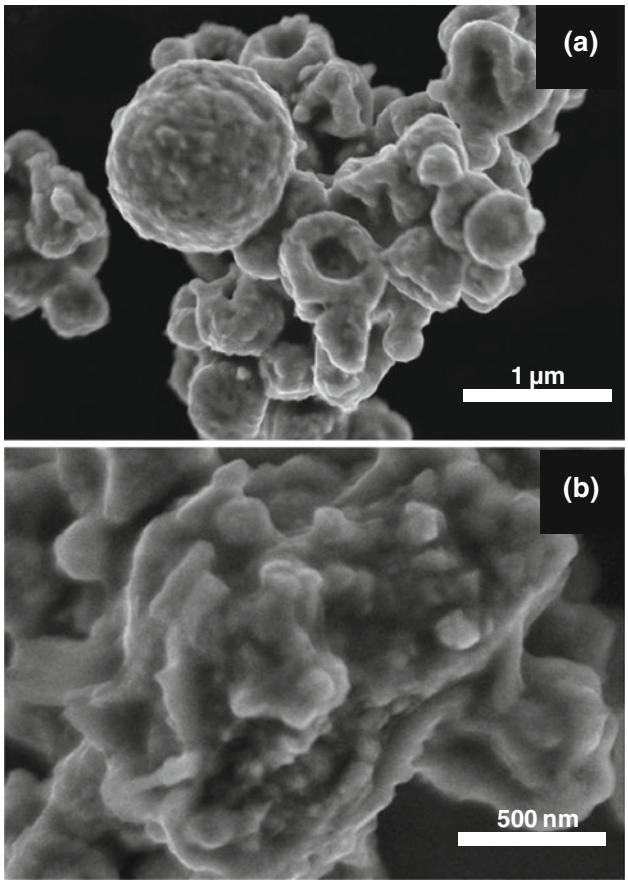

Fig. 2 FE-SEM images of the pseudo-spherical perovskites prepared by spray pyrolysis: **a** Representative micrograph for all the perovskites after annealing at 600 °C; **b** Detail of the micro-domains observed in the spherical particles

generally hollow pseudo-spherical particles with a wide variety of sizes from 150 to 2 μm (Fig. 2a). These particles are constituted by aggregates of smaller nanoparticles ca. 20–40 nm. Scherrer calculations (Table 1) and SEM images have shown that additional nano-crystalline domains of 30 nm are also formed throughout the surface of the bigger spherical particles (Fig. 2b).

3.2 O_2-TPD Experiments in Vacuum

The oxygen desorption profiles (TPD) of the $La_{1-x}Sr_xCoO_{3-\delta}$ perovskites series are shown in Fig. 3. Two consecutive TPD runs (denoted as TPD-1 and TPD-2) have been collected to determine the oxygen species directly associated with the perovskites and simultaneously track the presence of deleterious carbon species from ambient contamination or from segregated phases in the as-prepared samples. The second has been accomplished to elucidate if the surface structure of the catalysts are reversible upon re-oxidation. Therefore, the mass profile associated to oxygen ($m/z = 32$; Fig. 3a, b) and carbonates ($m/z = 44$; Fig. 3c, d) were monitored during the TPD experiments.

As we observed previously in some nickelites samples [15], the TPDs obtained for the cobaltite samples show three types of oxygen desorbing species (Fig. 3a, b). The lower temperature peak (usually denoted as α) for temperatures below 400 °C corresponds to oxygen adsorbed over surface anionic vacancies [1, 30, 31]. An intermediate peak (α') for the temperature range 400–700 °C has normally been ascribed to lattice oxygen as oxygen from dislocations and grain frontiers [1, 15, 30–33]. Recent X-ray photoemission studies carried out in our group [12] over lanthanum substituted cobaltites and by Rousseau et al. [22] over La–Co–Fe systems support this latter affirmation and point out to the presence of high binding energy species with low electron density. These oxygen species have a low coordination state and are likely associated to the presence of nearby cation vacancies and/or defects in the oxide structure [1, 12, 22, 30]. Therefore, it is important to correlate and determine the reactivity nature of this kind of species. The peak (denoted as peak β) at temperatures higher than 700 °C has been previously assigned to either lattice network oxygen from inner vacancies or oxygen directly produced by the reduction of metals in B positions [30, 31, 34].

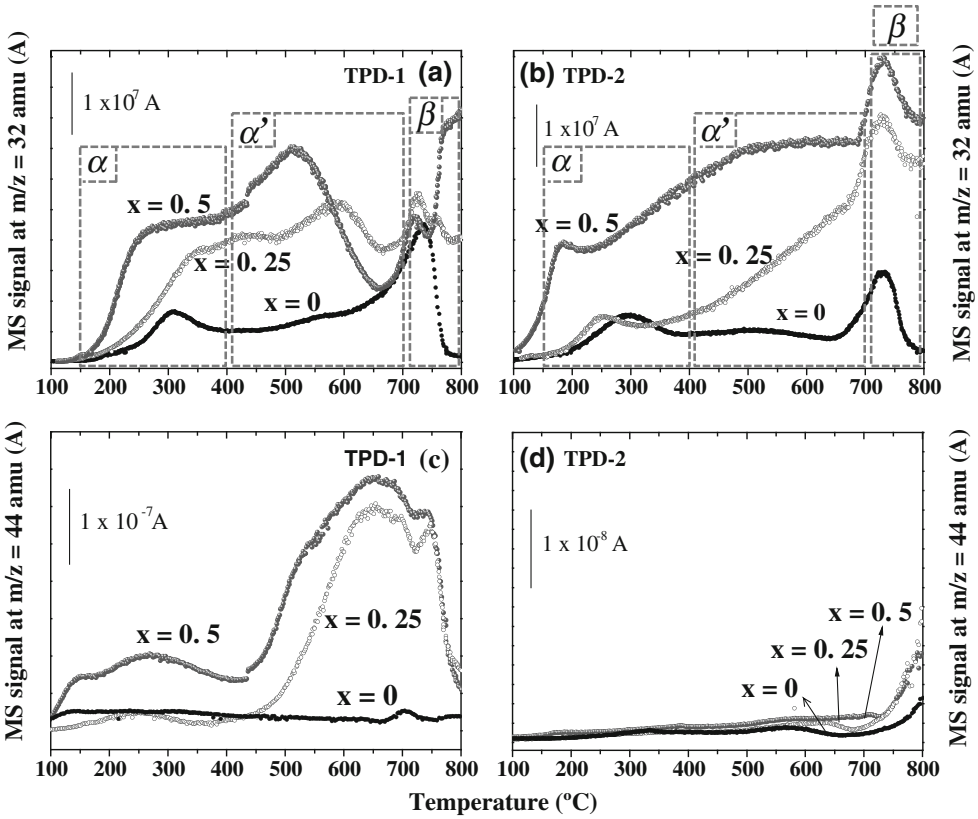

Fig. 3 TPD-O_2 profiles in vacuum determined for: $La_{1-x}Sr_xCoO_{3-\delta}$ systems corresponding to TPD-1 (**a**, **c**) and TPD-2 (**b**, **d**).Evolution of the mass spectra: $m/z = 32$ (**a**, **b**) and $m/z = 44$ (**c**, **d**)

Interestingly, in the $La_{1-x}Sr_xCoO_{3-\delta}$ series (Fig. 3a, b), the contribution from oxygen weakly chemisorbed species (α species at T < 400 °C) becomes more important with the Sr substitution, and oxygen species from boundaries or defects (α' species at 400 °C < T < 700 °C) can be easily distinguished as the strontium substitution increases. The total amount of oxygen desorbed per g of catalyst was calculated and it is shown in the Table 1. These data also reflect a higher desorption of oxygen in the samples substituted and show how the presence of Sr^{2+} cations improves the lability and the reactivity of some kinds of oxygen species in the perovskite structure.

In relation with the total amount of desorbed oxygen, the behaviour of the three samples are pretty different during the first and second TPD. In the case of the unsubstituted $LaCoO_3$, the total amount of oxygen decreases after the second TPD. On the contrary, the amount of O_2 desorbed is bigger after the TPD-2 for $La_{0.5}Sr_{0.5}O_{3-\delta}$ and equal for the $La_{0.75}Sr_{0.25}O_{3-\delta}$. Besides this changes, the distribution of the desorbed species are strongly modified in the samples with Sr. In general, a lower amount of α species (related with oxygen adsorbed over the surface) and a higher amount of β oxygen (related with oxygen species produced by the reduction of cobalt) are observed after the second TPD. These two process could be interrelated due to a higher amount of surface oxygen could protect or provide a "barrier" to avoid the desorption of inner oxygen species

$\mu mol_{O2}/g_{catal}$	TPD-1	TPD-2	TPD-3	TPD-4
$La_{0.75}Sr_{0.25}CoO_{3-\delta}$	236	236	229	214

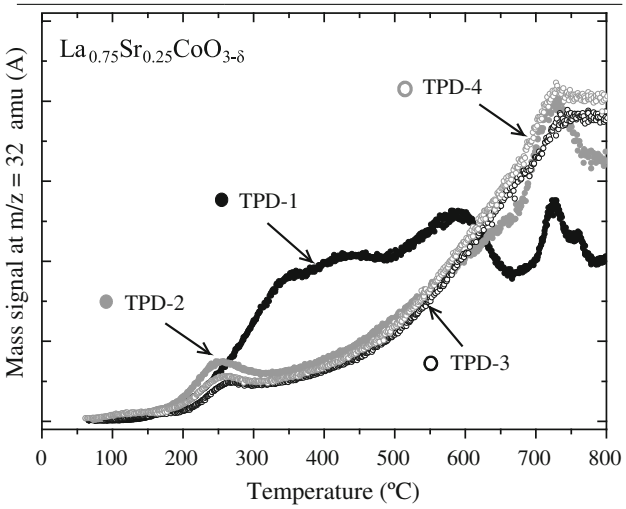

Fig. 4 TPD-O_2 profiles in vacuum determined for: $La_{0.75}Sr_{0.25}CoO_{3-\delta}$ systems corresponding to four consecutive TPDs (TPD-1, TPD-2, TPD-3 and TPD-4)

that reduce the cobalt. After a third and a fourth TPD (Fig. 4), for the intermediate sample ($La_{0.75}Sr_{0.25}O_{3-\delta}$) the amount of O_2 remains stable, what could be translate as a system stable after a second cycle, not only in the total amount of O_2 but also in the shape of the profile (Fig. 4).

After examining the evolution of $m/z = 44$ in Fig. 3c, d, it is apparent that the samples substituted with strontium present a remarkable bigger desorption of carbonate species from surface contamination or most probably, carbonates associated to lanthanum and especially strontium segregated species [12]. This surface carbonates disappear after the TPD-1 as we can conclude by the almost cero signal of mass 44 in all the samples in the TPD-2.

3.3 TPR-H_2 Experiments

TPR profiles corresponding to the lanthanum substituted cobaltites ($La_{1-x}Sr_xCoO_{3-\delta}$) are displayed in Fig. 5. In the case of the $LaCoO_3$ sample ($x = 0$), two major reduction steps can be identified. A low temperature reduction stage occurs between 370 and 450 °C, usually associated with the first reduction of cobalt from the trivalent to the divalent state [1, 15, 30, 31] which we have also recently confirmed by recent in situ XAS experiments [35]. The main H_2 consumption peak in this sample appears at higher temperatures and corresponds to the second reduction step where the perovskite and their respective oxides (produced in the first reduction step) are reduced to metallic cobalt. From the TPR profiles is clear that the introduction of Sr ($x = 0.5$) shifts this second peak to lower temperatures, reaching 450 °C in the $La_{0.5}Sr_{0.5}CoO_{3-\delta}$ sample, about 100 °C lower than the non-substituted cobaltite. The intermediate-substituted perovskite (Fig. 5, $x = 0.25$), shows also a very acute reduction peak at 575 °C, indicating a new kind of reduction process of cobalt. This lability effect of Sr is somehow similar to that previously observed for the Ni–Co samples [15, 36, 37] where the higher reducibility was found for the Ni 50 % sample.

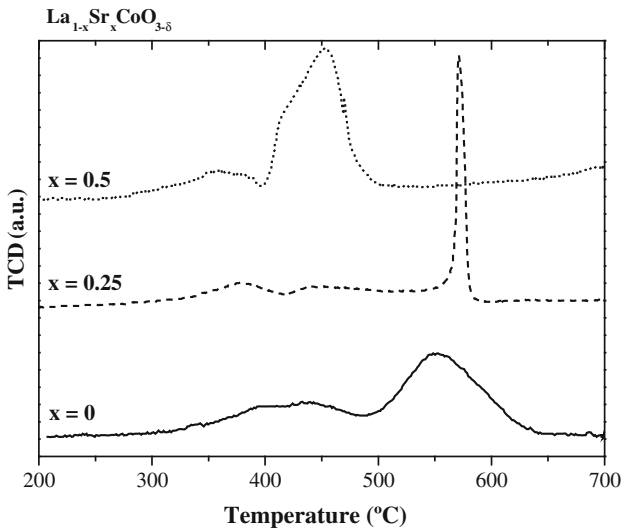

Fig. 5 TPR-H_2 profiles of: $La_{1-x}Sr_xCoO_{3-\delta}$ systems

3.4 Catalytic Oxidation of Toluene

The catalytic behaviour of perovskites containing Ni ($LaNi_{1-y}Co_yO_{3-\delta}$) was studied previously [15] and total oxidation of toluene was achieved in all the cases at temperatures below 400 °C. The samples containing cobalt exhibited better catalytic performance than the $LaNiO_3$, having the sample $LaCoO_3$ ($y = 1$) the best catalytic performance. The insertion of strontium in the sample with the best catalytic behaviour ($LaCoO_3$) slightly increases the catalytic performance in the deep oxidation of toluene as we describe as follows. Figure 6 shows the toluene conversion as a function of temperature for the lanthanum substituted cobaltites ($La_{1-x}Sr_xCoO_{3-\delta}$) showing that after 50 % substitution of La by Sr a slight enhancement in the catalytic properties is observed. Moreover, the performance achieved by the $La_{0.75}Sr_{0.25}CoO_{3-\delta}$ catalyst is the best at lower temperatures (T < 230 °C). As shown in Table 1, the comparison of the T_{50} conversion values for the three samples shows slight differences between the non-substituted and the Sr-doped perovskites, but the lower temperature corresponds to $La_{0.75}Sr_{0.25}CoO_{3-\delta}$, the sample with the higher Sr substitution (insert in Fig. 6). At higher temperature, with conversions higher than 80 %, the slope of the activity curve declines, being better the performance of the $La_{0.5}Sr_{0.5}CoO_{3-\delta}$ perovskite, which achieves total oxidation at 245 °C. These effects might be related with either a change in the oxidation mechanism [38] or the partial segregation of the perovskite phase in the presence of toluene at high temperatures [14].

4 Discussion

The substitution of Sr (II) for La (III) generates an electronic unbalance of the perovskite structure. To

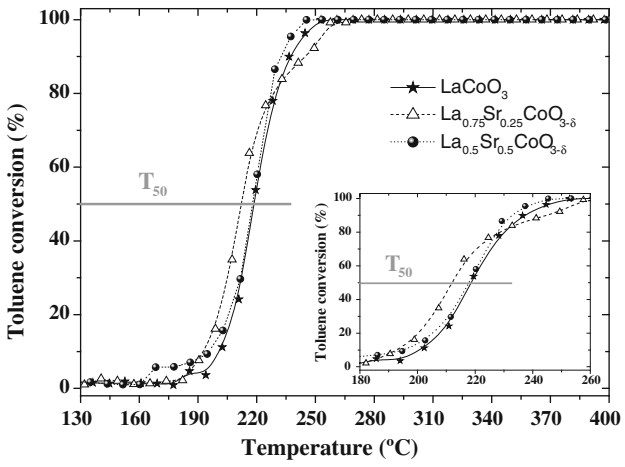

Fig. 6 Toluene conversion as a function of the reaction temperature on: $La_{1-x}Sr_xCoO_{3-\delta}$ system ($x = 0$, 0.25, 0.5). GSHV = 30,000 l kg^{-1} h^{-1}

compensate and preserve electroneutrality, two mechanisms are generally accepted: (i) an increase in the average oxidation state of Co^{3+} to Co^{4+} and (ii) the generation of oxygen vacancies. Recent X-ray absorption experiments carried out in our group point out to the latter as the most probable possibility since no significant shifts were found in the Co–K edge upon strontium substitution [35]. Moreover, the TPD-O_2 experiments shown in Fig. 3 further support with this assumption. The most weakly bonded oxygen species are desorbed at lower temperatures and are normally ascribed to oxygen adsorbed on anionic vacancies [31]. These species denoted as α-oxygen become predominant as the substitution degree is increased (c.f. Fig. 3).

The partial replacement of La by Sr also affects to the structural properties of the perovskites. We have recently explained by XAS and crystal field theory that the higher ionic radius of Sr(II) respect to La(III) (1.58 vs. 1.50 Å) modifies the rhombohedral structure of the $LaCoO_3$ and makes it evolve to the nearly cubic symmetry of the $La_{0.5}Sr_{0.5}CoO_{3-\delta}$ perovskite [35]. This fact has been also observed in analogous perovskite systems [30]. Additionally, the XRD results depicted in Fig. 1 show a progressive loss of crystallinity in the diffraction peaks with the Sr substitution. Therefore, not only a change of symmetry is produced, the mismatch of the cation size destabilizes and retards the formation of the final perovskite structure. The size of the crystalline domains calculated by the Scherrer equation further supports this hypothesis since a reduction from 32 nm in the non-substituted cobaltite to 13 nm in the $La_{0.5}Sr_{0.5}CoO_{3-\delta}$ is observed by XRD (see Table 1).

Other major effect normally associated with the partial substitution of cations in the A position deals with the increase of the mobility of oxygen through the anionic vacancies generated within the perovskite lattice [13, 17]. Our TPDs of oxygen have shown how the contribution of α′ species in the range of temperatures between 400 and 700 °C becomes more important with increasing Sr-doping (Fig. 3a). Therefore we can assume that the α′-oxygen desorbed species correspond to oxygen from structural defects such as dislocations or grain boundaries. Previous studies carried out by Royer et al. [31] suggest this possibility and recent XPS in situ experiments in our group also agree with this assignation [12]. These structural changes can be also responsible for the major susceptibility to reduction observed in TPR experiments for the $La_{0.5}Sr_{0.5}CoO_{3-\delta}$ perovskite (Fig. 5). Consequently, the main H_2 consumption peak generally associated to the reduction of lattice oxygen from the perovskite [7, 30, 31, 34] appears at 450 °C while the non-substituted $LaCoO_3$ shows that peak at 550 °C (Fig. 5).

Despite of all these changes observed in the structural and redox properties of the $La_{1-x}Sr_xCoO_{3-\delta}$ series the catalytic conversion activities obtained for the three samples are only slightly different (Fig. 6). Total toluene oxidation is achieved in all cases at T < 250 °C (see values in Table 1). The moderate reaction temperatures required to fully oxidize the toluene are again indicative of a suprafacial mechanism [15, 30] where the main contributing species are the weakly chemisorbed α and α′ oxygens. These toluene conversion levels are quite similar to those found in previous studies with nanometric Sr-cobaltites [21] or Pd-supported on lanthanum perovskites [39] and slightly better than other analogous perovskite systems prepared by conventional ceramic methods [5, 7, 19] or deposited on higher surface area supports [6, 24]. A closer comparison of catalytic performances can be made in terms of specific reaction rates respect to similar lanthanum-substituted perovskites working under similar experimental conditions (i.e. GHSV = 30,000 l kg^{-1} h^{-1} and O_2:toluene (1:400) ratios). In our case, the increasing substitution of strontium reduces the specific reaction rates at 220 °C from 16.2 to 7.5 × 10^{-9} mol of converted toluene per second and per square meter (Table 1), related with the higher specific surface area obtained for the Sr substituted systems. Nevertheless, our perovskites exhibit higher reaction rates than the La–Sr–Co systems prepared by Deng et al. [20] or the La–Sr–Co–Fe perovskites synthesized by Rousseau et al. [22] which are closer to 6 × 10^{-9} mol m^{-2} s^{-1}.

The lower activity found at high temperatures in the $La_{0.75}Sr_{0.25}CoO_{3-\delta}$ perovskite (Fig. 6 and insert for further details) can be attributable to the absence of a well-defined perovskite structure and the interference of some segregated phases. It is well-established that the formation of a homogeneous perovskite network is easier when an equivalent amount of La and Sr exists like in the $La_{0.5}Sr_{0.5}CoO_{3-\delta}$ case [14]. Nevertheless, the temperatures of 50 % conversion of toluene (T_{50}) remain rather close as shown on Table 1 and Fig. 6.

In order to compare the results obtained in this $La_{1-x}Sr_xCoO_{3-\delta}$ series with the previously studied $LaNi_{1-y}Co_yO_{3-\delta}$ samples, where the $LaNiO_3$ sample exhibited the lowest catalytic activity [15], different factors must be taken into account. For instance, the major specific surface area available in the $LaCoO_3$ perovskite (Table 1) or the possible deactivation of Ni sites due to the formation of carbonaceous species. It has been previously reported in steam and dry reforming studies of different catalytic systems containing Ni, that the progressive formation of carbon prevents the better performance of this type of catalysts [40–42]. Electron-filtered and FE-SEM images analysis of the perovskites after the reaction with toluene corroborate this statement. Amorphous carbon sheets are identified on the $LaNiO_3$ perovskite (Fig. 7b1, b2) while no rests are identified on any of the cobaltites (Fig. 7a1–b2). The presence of cobalt is preventing the formation of these

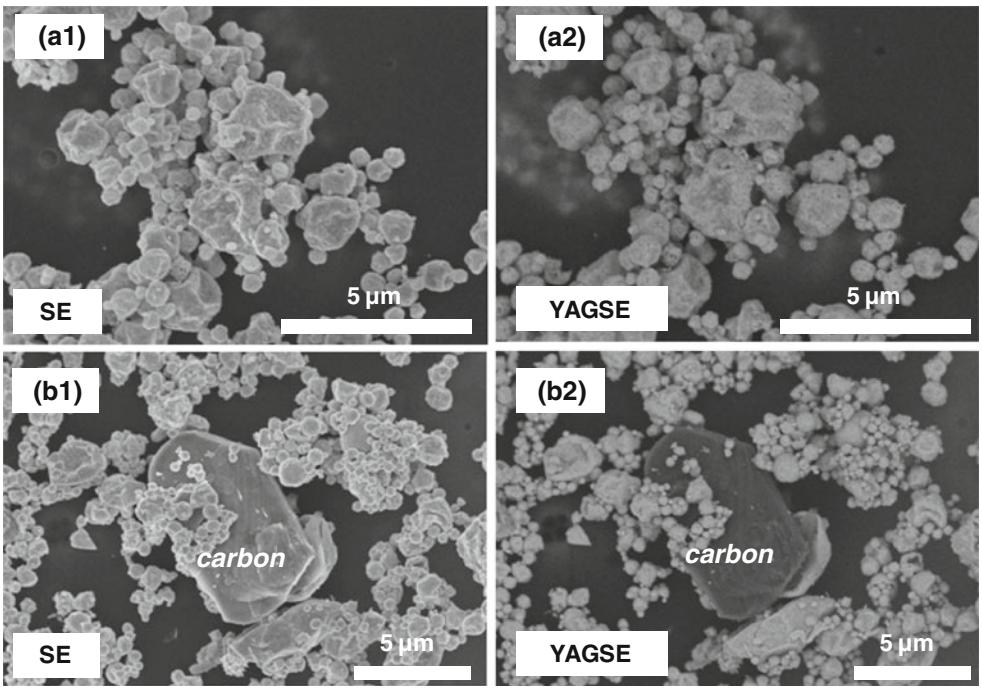

Fig. 7 FE-SEM images after reaction with toluene (1-SE and 2-YAGSE) of the samples: **a** $LaSr_{0.5}Co_{0.5}O_{3-\delta}$ and **b** $LaNiO_3$

carbonaceous species thereby maintaining a similar catalytic activity and specific reaction rates as found for the lanthanum substituted perovskites ($La_{1-x}Sr_xCoO_{3-\delta}$ series) (see values on Table 1). So, further FE-SEM and XRD analysis (not shown) of the cobaltites after reaction do not reveal significant structural changes or the appearance of carbonate species.

Therefore, we can conclude that the lanthanum substitute cobaltites are quite good and stable candidates for the deep oxidation of toluene, and that the partial substitution of La by Sr suppose a slight difference in catalytic activity, at least in our experimental conditions, although the higher mobility and lability of the substituted perovskite allow us to expect for beneficial effect in other oxidation reaction.

5 Conclusions

Different sets of lanthanum based perovskites prepared by a spray pyrolysis method have been tested in the deep oxidation of toluene yielding excellent conversion results at temperatures below 250 °C for all the samples evaluated. The progressive substitution in the A-site positions ($La_{1-x}Sr_xCoO_{3-\delta}$ system) provokes just a slight improvement on the final catalytic results, while the replacement in the B-sites in the $LaNi_{1-y}Co_yO_{3-\delta}$ series was determinant to further improve the total conversion yields. A suprafacial catalytic mechanism is suggested where the α-types oxygen species play an active role in the temperature range 230–400 °C. Finally, the best results for catalytic oxidation of toluene have been obtained for the cobalt-containing samples, being the $La_{0.75}Sr_{0.25}CoO_{3-\delta}$ a good option to reduce the temperature of reaction.

Acknowledgments We thank the Ministry of Science and Education of Spain for financial support (Projects ENE2004-01660 and ENE2007-67926-C02-01) and a PhD fellowship for R.P.).

References

1. Bialobok B, Trawczynski J, Mista W, Zawadzki M (2007) Appl Catal B Environ 72:395
2. Rodrigues ACC (2007) Catal Commun 8:1227
3. Spinicci R, Tofanari A, Faticanti M, Pettiti I, Porta P (2001) J Mol Catal A Chem 176:247
4. Spivey JJ (1987) Ind Eng Chem Res 26:2165
5. Chang C, Weng HS (1993) Ind Eng Chem Res 32:2930
6. Alifanti M, Florea M, Somacescu S, Parvulescu VI (2005) Appl Catal B Environ 60:33
7. Irusta S, Pina MP, Menendez M, Santamaria J (1998) J Catal 179:400
8. Okumura K, Kobayashi T, Tanaka H, Niwa M (2003) Appl Catal B Environ 44:325
9. Kubacka A, Fuerte A, Martinez-Arias A, Fernandez-Garcia M (2007) Appl Catal B Environ 74:26
10. Todorova S, Kadinov G, Tenchev K, Caballero A, Holgado JP, Pereñiguez R (2009) Catal Lett 129:149
11. Todorova S, Naydenov A, Kolev H, Holgado J P, Ivanov G, Kadinov G, Caballero A (2012) Appl Catal A Gen 413–414:43
12. Hueso JL, Caballero A, Ocaña M, González-Elipe AR (2008) J Catal 257:334

13. Nakamura T, Misono M, Yoneda Y (1982) Bull Chem Soc Jpn 55:394
14. Tejuca LG, Fierro JLG (1993) Properties and applications of perovskite-type oxides, vol 1. Marcel Dekker, New York
15. Pereñíguez R, Hueso JL, Holgado JP, Gaillard F, Caballero A (2009) Catal Lett 131:347
16. Peña MA, Fierro JLG (2001) Chem Rev 101:1981
17. Nakamura T, Misono M, Yoneda Y (1981) Chem Lett 10:1589
18. Agarwal DD, Goswami HS (1994) React Kinet Catal Lett 53:441
19. Liang JJ, Weng HS (1993) Ind Eng Chem Res 32:2563
20. Deng JG, Zhang L, Dai HX, He H, Au CT (2008) Ind Eng Chem Res 47:8175
21. Li N, Boreave A, Deloume JP, Gaillard F (2008) Solid State Ion 179:1396
22. Rousseau S, Loridant S, Delichere P, Boreave A, Deloume JP, Vernoux P (2009) Appl Catal B Environ 88:438
23. Blasin-Aube V, Belkouch J, Monceaux L (2003) Appl Catal B Environ 43:175
24. Alifanti M, Florea M, Parvulescu VI (2007) Appl Catal B Environ 70:400
25. López-Navarrete E, Caballero A, Orera VM, Lázaro FJ, Ocaña M (2003) Acta Mater 51:2371
26. Malet P, Caballero A (1988) J Chem Soc Faraday Trans 84:2369
27. Gaillard F, Joly JP, Perrard A (2007) Adsorpt Sci Technol 25:245
28. Gaillard F, Joly JP, Boreave A, Vernoux P, Deloume JP (2007) Appl Surf Sci 253:5876
29. Gaillard F, Joly JP, Li N, Boreave A, Deloume JP (2008) Solid State Ion 179:941
30. Merino NA, Barbero BP, Grange P, Cadus LE (2005) J Catal 231:232
31. Royer S, Berube F, Kaliaguine S (2005) Appl Catal A Gen 282:273
32. Jimenez VM, Espinos JP, Gonzalez-Elipe AR (1998) Surf Interface Anal 26:62
33. Jimenez VM, Fernandez A, Espinos JP, Gonzalezelipe AR (1995) J Electron Spectrosc Relat Phenom 71:61
34. Royer S, Alamdari H, Duprez D, Kaliaguine S (2005) Appl Catal B Environ 58:273
35. Hueso JL, Holgado JP, Pereñíguez R, Mun S, Salmeron M, Caballero A (2010) J Solid State Chem 183:27
36. Espinós JP, Gonzalez-Elipe AR, Caballero A, García J, Munuera G (1992) J Catal 136:415
37. Pereñíguez R, González-DelaCruz VM, Caballero A, Holgado JP (2010) Appl Catal B Environ 93:346
38. Hueso JL, Martínez-Martínez D, Caballero A, González-Elipe AR, Mun S, Salmerón M (2009) Catal Commun 10:1898
39. Giraudon JM, Elhachimi A, Wyrwalski F, Siffert S, Aboukais A, Lamonier JF, Leclercq G (2007) Appl Catal B Environ 75:157
40. Sierra Gallego G, Batiot-Dupeyrat C, Barrault J, Florez E, Mondragón F (2008) Appl Catal A Gen 334:251
41. Vaz T, Salker AV (2007) Mater Sci Eng B Adv Funct Solid State Mater 143:81
42. González-DelaCruz VM, Holgado JP, Pereñíguez R, Caballero A (2008) J Catal 257:307